Global Retrospective Estimation of Soil Moisture Using the Variable Infiltration Capacity Land Surface Model, 1980–93

BART NIJSSEN, REINER SCHNUR,* AND DENNIS P. LETTENMAIER

Department of Civil and Environmental Engineering, University of Washington, Seattle, Washington

(Manuscript received 10 December 1999, in final form 14 July 2000)

ABSTRACT

A daily set of surface meteorological forcings, model-derived surface moisture fluxes, and state variables for global land areas for the period of 1979–93 is described. The forcing dataset facilitates global simulations and evaluation of land surface parameterizations without relying heavily on GCM output. Daily precipitation and temperature are based on station observations, daily wind speeds are based on National Centers for Environmental Prediction–National Center for Atmospheric Research reanalysis data, and the remaining meteorological forcing variables (shortwave radiation, longwave radiation, and vapor pressure) are derived from the precipitation and temperature series. The Variable Infiltration Capacity (VIC) land surface model is used to produce a set of derived fluxes and state variables, including snow water equivalent, evapotranspiration, runoff, and soil moisture storage. The main differences between the new dataset and other, similar datasets are the daily time step, the use of a specified simulation period as opposed to climatological averages, the length of the simulation period, the use of observed meteorological data, and the use of a more realistic hydrological model. Comparison with observations and existing climatologies shows that 1) the interannual variation in simulated snow cover extent is similar to observations in Eurasia but is somewhat underpredicted in North America; 2) the components of the global and continental water balance are similar to those in previously produced climatologies, although runoff is somewhat lower; 3) patterns of simulated soil moisture storage are similar to the climatology of Mintz and Serafini, but the more sophisticated VIC hydrological model produces a larger range in soil moisture; and 4) the annual cycle and spatial patterns in soil moisture compare well with soil moisture observations in Illinois and in central Eurasia, but mean modeled soil moisture is somewhat lower than observed, and observed soil moisture shows a greater interannual persistence than do the simulations.

1. Introduction

Water stored as soil moisture forms only a very small fraction of the water reserves on the planet—about 0.001% of total water reserves and 0.05% of freshwater reserves (Dingman 1994). However, the availability of soil moisture at any given time or place plays an important role in the exchange of moisture and energy between the atmosphere and the land surface. Numerical model studies have clearly shown the sensitivity of model-simulated climates to the specification of soil moisture and/or its effects on vegetation evaporative stress, both at a regional and global scale (e.g., Koster and Suarez 1995; Koster et al. 2000; Mintz 1984). Soil moisture availability affects the partitioning of incoming energy into convective latent and sensible heat fluxes (Betts et al. 1996). It also affects the thermal properties of the soil (Dirmeyer et al. 1999) as well as surface albedos, since wetter soils tend to be darker (Robock et al. 1998).

One of the problems in modeling and verifying simulated soil moisture in global climate simulations is the lack of a good observational database, which hampers efforts to improve model physical representations (Dirmeyer 1995). Datasets of observed soil moisture are generally limited in their spatial extent or the time period they cover. However, a number of regional datasets exist (e.g., Hollinger and Isard 1994; Vinnikov and Yeserpova 1991) that have been used for comparison with model-simulated soil moisture (Robock et al. 1998). The dataset most often used for initialization of general circulation models (GCMs) for climate simulation and weather prediction is a monthly climatology of soil moisture and evapotranspiration generated by Mintz and Serafini (1992) in the early 1980s using a simple water budget approach based on Thorntwaite and Mather (1955). They calculated the monthly available soil moisture and evapotranspiration based on monthly mean climatologies of precipitation and surface air temperature.

* Current affiliation: Max-Planck-Institut für Meteorologie, Hamburg, Germany.

Corresponding author address: Dennis P. Lettenmaier, Dept. of Civil and Environmental Engineering, Box 352700, University of Washington, Seattle, WA 98195-2700.
E-mail: dennisl@u.washington.edu

The budget calculations accounted for evaporation from interception storage, evaporation from the soil, and transpiration by the vegetation. All precipitation was treated as rainfall, and rainfall in excess of total evapotranspiration entered the soil column. When the soil column reached field capacity, any rainfall in excess of evapotranspiration would contribute to runoff. Maximum allowed storage in the soil column was 150 mm. Similar datasets have been produced by Willmott et al. (1985), who used a different source for meteorological data and (Levis et al. 1996), who used a more sophisticated hydrological model to produce a monthly global climatology of soil moisture. Schemm et al. (1992) simulated monthly soil moisture for the period 1979–89, using a similar methodology as Mintz and Serafini (1992), but with monthly varying precipitation and temperature. Liston et al. (1993) produced a daily time series of soil moisture, evapotranspiration, and runoff at a resolution of $4^\circ \times 5^\circ$ for the period 1979–88 using a version of the Simplified Simple Biosphere Model. Observed average monthly precipitation was disaggregated into daily data by scaling the monthly time series by the frequency of observed 1979 daily precipitation events. Both Schemm et al. and Liston et al. treated all precipitation as rainfall and consequently did not take snow into account.

The past two decades have seen a rapid growth in the development of land surface schemes that model the interaction between the atmosphere, the land surface, and the near-surface hydrological cycle. Recently, three model intercomparison studies have been conducted that evaluated soil moisture simulations for a number of land surface parameterizations.

The Project for Intercomparison of Land Surface Parameterization Schemes (PILPS) (Henderson-Sellers et al. 1995, 1993) used offline simulations to examine the overall performance of land surface schemes both for point locations (e.g., Schlosser et al. 2000) and for the Arkansas–Red River Basin in the Southern Great Plains region of the United States (Liang et al. 1998; Lohmann et al. 1998a; Wood et al. 1998). In the Arkansas–Red River simulations [PILPS 2(c)] the land surface models were forced with observed meteorological data for a period of 10 yr (1979–88).

The Global Soil Wetness Project (GSWP) was designed to provide improved global soil moisture fields for use in GCMs (Dirmeyer et al. 1999). These fields can be used for initialization, as a lower boundary condition, or as a check on GCM-simulated soil moisture fields. The land surface schemes were forced with observed precipitation and European Centre for Medium-Range Weather Forecasts (ECMWF) reanalysis temperature, which allows more straightforward evaluation of the land surface schemes than in fully coupled runs in which surface hydrological behavior is forced with model-generated meteorological conditions. The model period for the GSWP pilot phase was limited to 1987–88 (Dirmeyer et al. 1999), using a $1^\circ \times 1^\circ$ spatial resolution. Soil and vegetation parameters for this study were largely based on the land surface datasets published as part of the International Land Surface Climatology Project Initiative I CD-ROM (Meeson et al. 1995; Sellers et al. 1992).

The Atmospheric Model Intercomparison Project (AMIP) conducted simulations with 30 atmospheric GCMs for the same 10-yr period as PILPS 2(c) (1979–88). The models were forced by observed sea surface temperatures, but the land surface schemes were fully coupled. Consequently, the surface hydrological behavior was driven by model-generated precipitation, surface temperature, and radiation, and simulated soil moistures were allowed to feed back on themselves (Robock et al. 1998). One difficulty in interpreting the AMIP soil moisture simulations is that the simulated soil moisture fields reflect not only the shortcomings of the land surface schemes used by each of the GCMs, but also differences in the atmospheric physics among the GCMs, especially related to precipitation.

In all of the model intercomparison studies, a rather large spread exists between the model results with respect to simulated mean soil moistures. In most cases simulated evapotranspiration agrees better than simulated soil moisture. In the few instances where observed soil moisture fields were available, the differences between the models were generally as large or larger than the differences between model simulations and observations (Entin et al. 1999; Lohmann et al. 1998a), even though most land surface schemes mirror the observed soil moisture changes qualitatively.

This paper consists of three parts. First, a new gridded dataset of global surface forcing variables is described. The core of this dataset consists of daily precipitation and daily minimum and maximum temperatures for the period 1979–93 for $2^\circ \times 2^\circ$ grid cells over the global land areas, excepting Antarctica and Greenland. In addition, the dataset contains vapor pressure, downward shortwave radiation, and net longwave radiation, derived from the daily temperature and precipitation data using standard algorithms. Daily wind speeds for each of the grid cells are based on the National Centers for Environmental Precipitation–National Center for Atmospheric Research (NCEP–NCAR) reanalysis project (Kalnay et al. 1996). This dataset is applicable to any offline application of land surface schemes. Second, a global dataset of derived variables is presented. These derived variables, which include soil moisture storage, evapotranspiration, runoff, and snow water equivalent, were computed by applying the forcing variables to the Variable Infiltration Capacity (VIC) model (Liang et al. 1994). Although the spatial resolution of the simulations is coarser than the GSWP simulations, the model period spans a period of 15 yr rather than 2 yr. The third part of the paper interprets the model results. The main differences between the new data and other, similar datasets are the daily time step, the use of a specified simulation period as opposed to climatological averages, the length

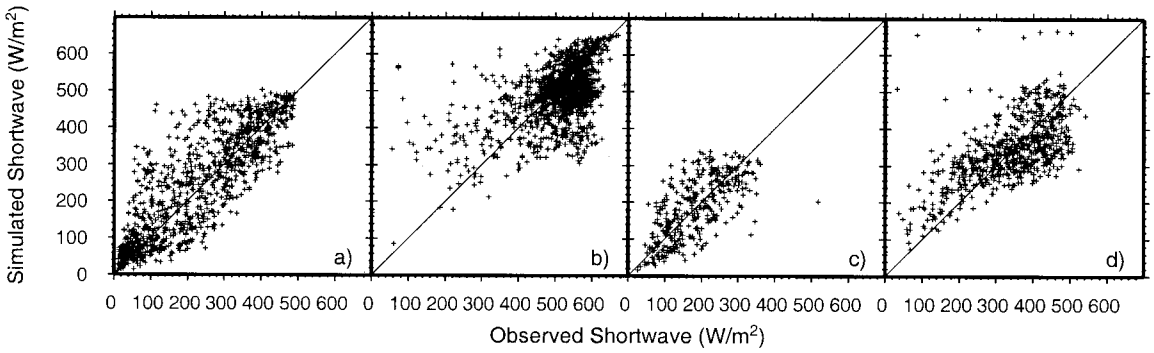

FIG. 1. Observed and simulated daily incoming shortwave radiation at selected sites. (a) Boreal forest in central Canada (BOREAS; Goulden et al. 1997); (b) Sahel region (HAPEX; Montény et al. 1997); (c) Prudhoe Bay, Alaska (Kane et al. 1997); (d) Rain forest in central Amazon (ARME; Shuttleworth et al. 1984). Simulated shortwave radiation according to Thornton and Running (1999).

of the simulation period, the compilation of meteorological forcings for this time period based on observations, and the use of a more realistic hydrological model.

2. Model forcing dataset

a. Meteorological forcing variables

One of the problems in modeling the hydrological behavior of large land areas for extended periods is the lack of meteorological observations with which to force the model simulations. Ideally, land surface schemes should be driven with observations of temperature, precipitation, wind, vapor pressure, and downward longwave and shortwave radiation. Unfortunately, only temperature and precipitation are measured routinely at a reasonably large number of locations around the world. Some of the meteorological variables can be measured through satellite remote sensing for large areas and at regular intervals, but these observations are available only for the recent past. Another possible source of forcing data is the output from atmospheric GCMs, but the biases in these models, particularly for precipitation, are generally still too large to allow direct application of GCM output in hydrological models (e.g., Leung et al. 1999).

One approach to dealing with this problem is to calculate the less well-known variables (vapor pressure, incoming shortwave radiation, and longwave radiation) as a function of daily precipitation and daily minimum and maximum temperature. Although this method has shortcomings, it allows the development of forcing datasets for historic periods, and all variables are calculated in a consistent manner. This approach has been adopted for this study.

Kimball et al. (1997) describe a regression method for dewpoint temperature, which uses the observed minimum temperature, annual precipitation, and an estimate of net radiation. The estimated dewpoint temperature can then be used to calculate vapor pressure. Thornton and Running (1999) describe a method for calculating downward surface shortwave radiation based on the daily temperature range and the dewpoint temperature. They modified the algorithm by Bristow and Campbell (1984) to cover a wider range of climatic regions. Because the Kimball et al. (1997) method for estimating dewpoint temperature requires an estimate of downward surface radiation and the Thornton and Running (1999) method for estimating downward shortwave radiation requires an estimate of dewpoint temperature, an iterative scheme was used to solve for both variables, as suggested by Thornton and Running (1999).

Thornton and Running (1999) tested their formulation for most climatic zones in the United States and found a mean absolute error of 27.7 W m^{-2} (14.9%) and a bias of 5.9 W m^{-2} (4.3%) for daily data at 40 stations. Mean absolute errors and biases at individual stations were significantly larger. The mean absolute error was largest in absolute terms at Miami, Florida (45 W m^{-2} or 22.9%) and largest in relative terms at Albany, New York (39 W m^{-2} or 35.4%). The bias was largest in absolute terms at Cape Hatteras, North Carolina (−38 W m^{-2} or −16.8%) and largest in relative terms at Albany, New York (29 W m^{-2} or 26.5%). Thornton and Running (1999) note specifically that their validation datasets, which are all within the continental United States do not include tropical or high-latitude climates. Therefore, we tested the method for additional sites in the Sahel [Hydrological Atmospheric Pilot Experiment (HAPEX)] (Goutorbe et al. 1997; Montény et al. 1997), the Amazon [Amazonian Region Micrometeorological Experiment (ARME)] (Shuttleworth et al. 1984), the boreal forest in central Canada [Boreal Ecosystem–Atmosphere Study (BOREAS)] (Goulden et al. 1997), and the North Slope of Alaska (Kane et al. 1997). All sites showed a somewhat larger scatter (Fig. 1), with mean absolute errors of 64 W m^{-2} or 12.7% (Sahel), 66 W m^{-2} or 20.2% (Amazon), 60 W m^{-2} or 26.5% (boreal forest), and 50 W m^{-2} or 27.1% (Alaska), respectively. The mean bias for each of the sites was −13 W m^{-2} or −2.5% (Sahel), 10 W m^{-2} or 2.9% (Amazon), 17 W

m^{-2} or 7.4% (boreal forest), and 4 W m^{-2} or 2.2% (Alaska).

Net longwave radiation at the surface was calculated according to Bras (1990) as a function of air temperature, humidity, and atmospheric transmittivity (from Thornton and Running 1999). The latter is used to calculate an equivalent cloudiness. Net longwave radiation was included in the dataset instead of incoming longwave radiation, because the VIC model does not calculate the land temperature when operated in water balance mode [see section 3a(5)].

No obvious relationships exist between air temperature or precipitation and wind speed. Surface measurements of wind speed are sparse and biased toward certain geographical settings (e.g., airports and hence flat local terrain). Interpolation of wind speed observations will generally not provide a reliable representation of wind speed variations over large areas. Instead, we estimated daily wind speeds from NCEP–NCAR reanalysis data (Kalnay et al. 1996), which are complete (daily averages) from 1948 to 1998 on a T62 Gaussian grid (approximately 1.9° × 1.9°) as separate u wind and v wind vectors. These wind vectors, which are for a 10-m measurement height, were linearly interpolated to the centers of each 2° × 2° cell to create a daily dataset of wind speed for each grid cell.

b. Daily temperature and precipitation dataset

Estimates of gridded monthly precipitation (Huffman et al. 1997; Hulme 1995) and temperature (Jones 1994) have been produced by recent studies for the global land surface. However, on a daily timescale only station observations or modeling results are available. To develop a gridded meteorological forcing dataset with a daily time step, the gridded monthly estimates of precipitation and temperature had to be disaggregated to a daily time step, reproducing the intermonthly statistics and spatial correlations as realistically as possible. Because of the problems inherent in the reanalyses data, especially for precipitation, station data were used instead, and a three-step procedure was applied in this study (Fig. 2).

As a first step, global station observations (about 7800 stations) from the Climate Prediction Center (CPC) were used to compute daily areal precipitation and daily minimum and maximum temperature over land. The CPC forms part of NCEP. The CPC Summary of Day data were derived from 3-hourly synoptic reports from the stations contributing to the Daily World Meteorological Data Network of the World Meteorological Organization. For each 2° × 2° grid cell, daily areal precipitation was computed from the available stations in that cell using a three-step procedure. First, the 2° × 2° grid cell was subdivided into 16 0.5° × 0.5° subcells. Second, the precipitation for each of the subcells was calculated as the weighted mean of all stations in the larger 2° × 2° grid cell. Inverse distance-squared weights were calculated based on the distance from each station to the center of each 0.5° × 0.5° subcell. Last, the precipitation values for the 16 subcells were averaged to derive an overall mean areal precipitation for the 2° × 2° grid cell. This procedure is equivalent to taking the weighted average of all stations in the 2° × 2° grid cell, where the weight for each station is the arithmetic average of the inverse distances squared from that station to the centers of each of the 16 0.5° × 0.5° subcells (see Smith 1993).

Minimum and maximum temperatures were averaged after lapsing each station to the mean grid cell elevation using a lapse rate of 0.0065°C m^{-1}. All stations in a cell were used and, in addition, at least two stations were required for precipitation. If, on a given day, observations were not available for a certain cell, a search for additional stations was performed within a radius of 150 km from the center of that cell.

Station coverage is best in North America, Europe, Japan, and parts of the former Soviet Union and China. However, data coverage is very sparse for large parts of the globe, particularly in central Australia, northern Canada, the Sahara, the Amazon Basin, and parts of Siberia. A simple spatial interpolation of daily data is inappropriate because of the spatial variability and the spatial correlation structure, especially for precipitation. Therefore, in data sparse regions where the first step was not successful, stochastic precipitation and temperature models were used to generate missing daily grid cell values. The precipitation model for this second step consisted of a two-state (wet/dry) first-order Markov chain for precipitation occurrences and a two-parameter gamma distribution for intensities (Geng et al. 1986). A first-order autoregressive model was used for minimum and maximum temperature anomalies (Nicks and Harp 1980). The parameters of these models were initially estimated from the data generated in the first step and then interpolated to land cells with missing data. Separate parameters were calculated for each month and in the case of temperature for each of the four possible transitions in rain state.

The daily temperature sequences from the first two steps were scaled to the monthly averages from Jones's monthly temperature data (Jones 1994) after interpolation of this dataset from a spatial resolution of 5° × 5° to 2° × 2°. The precipitation dataset was scaled in two stages using monthly time series from two different sources. The Global Precipitation Climatology Project (GPCP) (Huffman et al. 1997) provides monthly precipitation data with global coverage at a 2.5° × 2.5° resolution starting in 1987. The Hulme (1995) dataset covers a longer time period, but has a coarser spatial resolution (3.75° × 2.5°). For this study, the GPCP monthly time series was used as the primary series. For the period 1987–93, the daily precipitation sequences were scaled to the monthly precipitation totals provided by GPCP, after interpolation of the GPCP precipitation to a 2° × 2° resolution. The Hulme (1995) precipitation dataset was interpolated from 3.75° × 2.5° to 2° × 2°

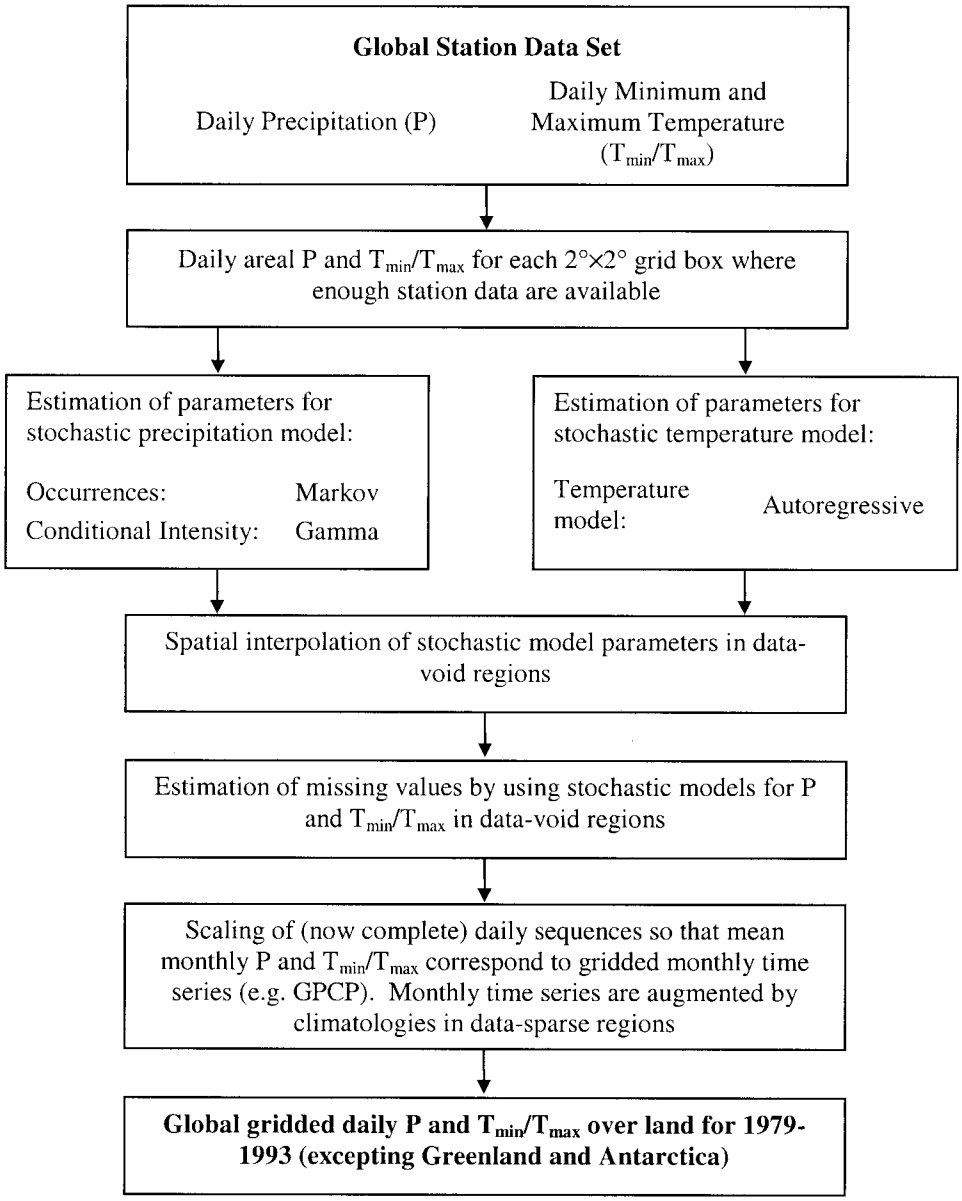

FIG. 2. Procedure for constructing the daily precipitation (P) and minimum (T_{min}) and maximum (T_{max}) temperature dataset. See section 2b for details.

and then used to scale the remainder of the series (1979–86). However, to avoid a change in precipitation characteristics between the first and second part of the time series, mean monthly scaling factors were calculated for each month for each grid cell for the coincident period (1987–93) between the GPCP and Hulme dataset. Last, the daily precipitation values during 1979–86 were multiplied by these scaling factors to construct a 15-yr precipitation series consistent with the GPCP monthly estimates. For those data-sparse regions where no monthly time series were available for the period of interest (1979–93), climatological monthly means were used. For temperature, a monthly climatology by P. D. Jones (1995, personal communication) was used, and the climatology by Legates and Willmott (1990) was used for precipitation.

By using all available stations from the CPC dataset, the first step ensured that the intramonthly probability distributions of the daily data and their spatial correlations are as realistic as possible. The second step was used only for cells for which no station observations were available. Thus for the most part, the generated daily sequences are based on observations, whereas in data-sparse regions at least their temporal probability distributions should be realistic. The values estimated stochastically are, of course, difficult to verify due to

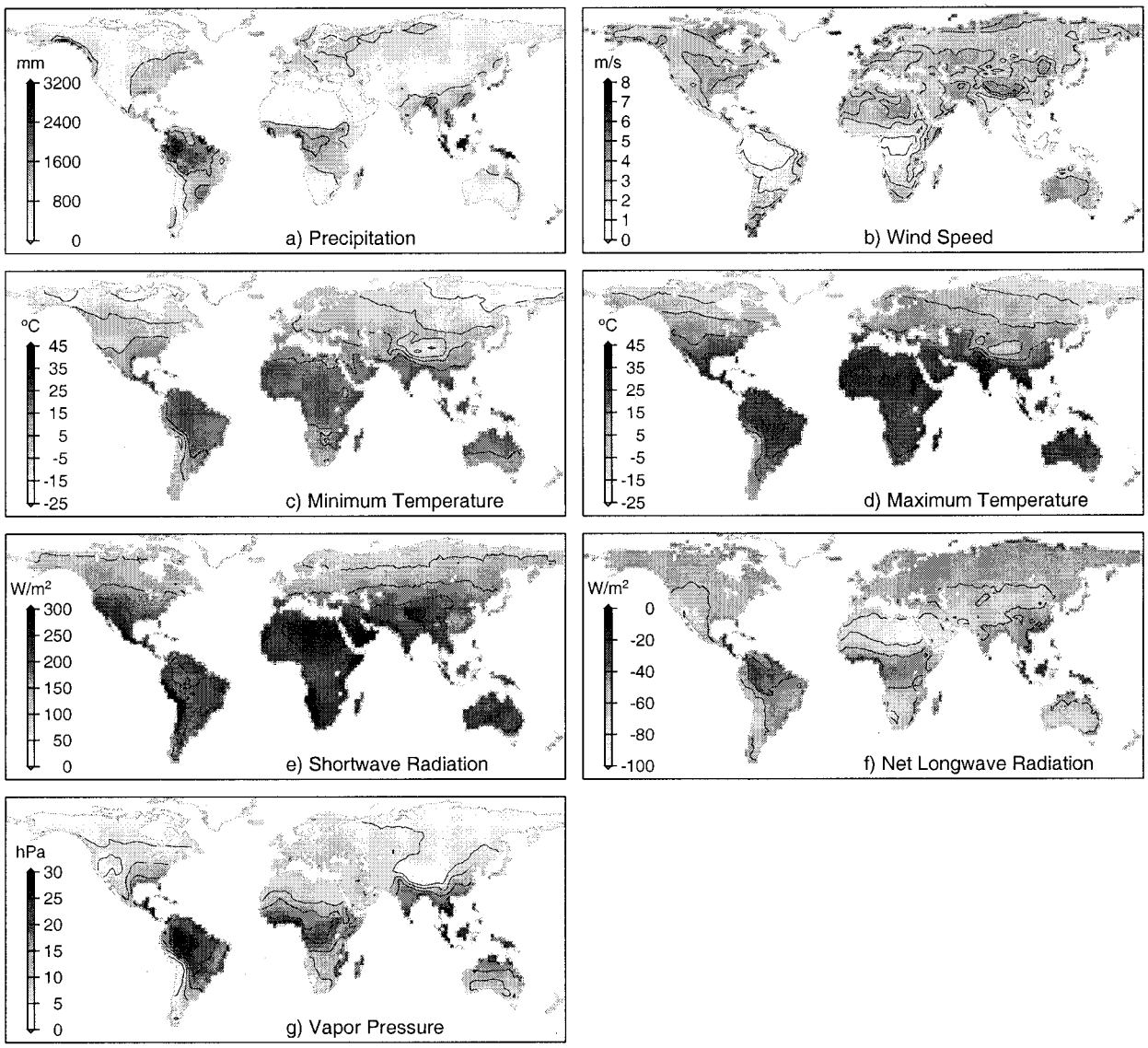

FIG. 3. Global fields of forcing variables (1979–93): (a) mean annual precipitation (mm), (b) mean wind speed (m s^{-1}), (c) mean daily minimum temperature (°C), (d) mean daily maximum temperature (°C), (e) mean incoming shortwave radiation (W m^{-2}), (f) mean net longwave radiation (W m^{-2}), (g) mean daily vapor pressure (hPa). Contours correspond to the ticks on the shading bar.

the lack of observations, which was the very reason for the use of this procedure. The third step ensured that the monthly values of the compiled product have undergone maximum quality checking. Figure 3 displays the global patterns of the variables in the forcing dataset (daily precipitation, wind speed, minimum and maximum temperature, incoming shortwave radiation, net longwave radiation, and vapor pressure). The monthly means of precipitation and temperature are identical to the best available datasets of monthly observations, while the use of station observations for disaggregation from monthly to daily ensures reasonably realistic intramonthly statistics.

3. Model-derived variables

The forcing dataset developed in section 2 can be used to drive any land surface scheme. In this section we describe use of the dataset to force the VIC model to produce a set of derived variables for the global land areas for the period 1980–93. These derived variables are evapotranspiration, runoff, soil moisture storage, and snow water equivalent.

a. Variable Infiltration Capacity model

The VIC model is described in detail elsewhere (e.g., Liang et al. 1996, 1994; Nijssen et al. 1997) and only

a short overview will be provided here. The VIC model is a macroscale hydrological model that has been used for a number of modeling studies of large-scale river basins (e.g., Abdulla et al. 1996; Lohmann et al. 1998c; Maurer et al. 2000; Nijssen et al. 1997; Wood et al. 1997). Its distinguishing characteristics include the representation of

- subgrid variability in land surface vegetation classes;
- subgrid variability in soil moisture storage capacity as a spatial probability distribution;
- subgrid variability in topography through the use of elevation bands;
- drainage from the lower soil moisture zone (base flow) as a nonlinear recession;
- spatial subgrid variability in precipitation.

Each of these elements is described briefly below.

1) VEGETATION

Variations in vegetation within a grid cell are described by specifying a given number of land cover classes and the fraction of the grid cell covered by each. The subsurface is characterized in the vertical direction by an arbitrary number of soil layers. For most applications two or three soil layers have been used. For each land cover (vegetation) class, the leaf area index (LAI), canopy resistance, and relative fraction of roots in each of the soil layers is specified. Evapotranspiration from each vegetation type is calculated using a Penman–Monteith formulation (Liang et al. 1994).

The moisture fluxes between the soil layers, and the evapotranspiration and runoff, vary with each vegetation class. Evapotranspiration, surface runoff and base flow are computed for each cover type and summed over all cover types within a grid cell weighted by the fractional area that each cover type occupies.

2) SOIL MOISTURE AND RUNOFF GENERATION

The subgrid-scale variability in soil properties is represented by a spatially varying infiltration capacity. Thus, the spatial variability in soil properties at scales smaller than the grid scale is represented statistically, without assigning infiltration parameters to specific subgrid locations. The infiltration curve can also be interpreted to represent the fraction of a grid cell that contributes runoff via ''fast'' response mechanisms, such as saturation excess or fast subsurface flow.

Drainage between the soil layers is modeled as gravity driven, with the unsaturated hydraulic conductivity a function of the degree of saturation of the soil (Campbell 1974). The deepest soil layer produces base flow according to the ARNO model base flow formulation (Todini 1996). In this way, the model separates subsurface flow from quick storm response.

The VIC model is coupled to a linear streamflow routing scheme. In essence, the routing model describes the time of concentration for runoff reaching the outlet of each grid cell as well as transport of water in the open channel system. All runoff exits the grid cell in only one of eight possible directions. This volume is then added to the water routed through the river channel system (Lohmann et al. 1996, 1998b).

3) ELEVATION BANDS

In mountainous areas, temperature and precipitation vary with elevation. This leads to subgrid variations in snow accumulation. To account for this effect, the VIC model subdivides each grid cell into a number of elevation bands. In this study, precipitation was assumed to be constant with elevation within a grid cell, but air temperature was lapsed from the mean grid cell elevation to the mean elevation of each elevation band using a lapse rate of $0.0065^{\circ}\text{C m}^{-1}$.

4) SPATIALLY VARIABLE PRECIPITATION

The subgrid spatial variability in precipitation is modeled according to Liang et al. (1996). The areal fraction of a model cell that experiences precipitation increases with increasing intensity of the precipitation event. The parameter relating precipitation intensity to areal extent of the precipitation event is a function of grid cell size, storm type, geography, and other factors (Fan et al. 1996).

5) SNOW COVER

The effect of vegetation cover on snow accumulation and melt is represented internally within the VIC model via a coupled snow model (Storck and Lettenmaier 1999). The snow model allows snow to be intercepted by the canopy, to fall through it, or to completely cover low vegetation or bare areas. Snow intercepted by the vegetation canopy can be removed via sublimation, meltwater drip, and mass release. Drip from the canopy is added to the ground snowpack as rain, while mass release is added as additional snowfall. Rain and snow interception by the canopy is calculated as a function of LAI. LAI is also used to attenuate shortwave radiation and wind passing through the canopy. The ground surface snow cover is modeled using a two-layer energy balance approach.

Precipitation is partitioned into rain and snow as a function of the air temperature. The fraction of the precipitation falling as rain or snow varies linearly between a rain and a snow threshold. When the air temperature is above the snow threshold, all precipitation falls as rain, when it is below the rain threshold all precipitation falls as snow. In this study the rain threshold was set to -0.5°C, and the snow threshold was set to $+1.5^{\circ}\text{C}$.

The VIC model can be operated in two modes. One mode is an energy balance mode in which all water and

energy fluxes near the land surface are calculated. The surface energy balance is closed by iterating on an effective surface temperature. In this case the model time step is typically from 1 to 3 h. The second mode is a water balance mode, which focuses on the water balance at the land surface, and uses approximations for the relevant energy terms. The most important of these is that the effective surface temperature is set equal to the air temperature. In this case the model is typically run at a daily time step, except when snow is present. When snow is present or when snowfall occurs, the daily meteorological forcings are disaggregated to hourly values and the model is run in energy balance mode to resolve the energy fluxes near the snow surface. Hourly temperatures are estimated by fitting a spline function using Hermite polynomials to the time series of daily minimum and maximum temperatures. Daily shortwave radiation is disaggregated based on the hourly potential solar radiation. Precipitation totals are spread evenly throughout the day.

b. Land surface characteristics

For each $2^\circ \times 2^\circ$ grid cell, land surface characteristics such as elevation, soil, and vegetation need to be specified. Although multiple vegetation types are allowed for each grid cell, only one set of soil parameters is specified for each.

1) TOPOGRAPHY

Elevation data were calculated based on the 5-min global Terrainbase Digital Elevation Model (Row et al. 1995), using the land surface mask from Graham et al. (1999). The mean elevation for each elevation band was calculated as the area-weighted mean of the 5-min land cells that fell into that band. A fixed elevation interval of 500 m was used for the elevation bands. A minimum threshold of 1% of the land area in a grid cell was used to limit the number of elevation bands. If a band contained less than 1% of the land area, the area was added to the neighboring elevation band with more than 1% of the grid cell land area. The maximum number of elevation bands per grid cell was 12, for the cell centered at 27°N, 87°E (East Nepal, Northeast India, North Bangladesh). The total number of model grid cells was 3462.

2) SOILS

Soil textural information and soil bulk densities were obtained using the Soilprogram (Carter and Scholes 1999), which combines the 5-min Food and Agricultural Organization–United Nations Educational, Scientific, and Cultural Organization (FAO–UNESCO) digital soil map of the world (FAO 1995) with the World Inventory of Soil Emission Potentials (WISE) pedon database (Batjes 1995). The digital soil map of the world records the soil type for each 5-min cell, while the WISE database contains soil attributes for a large number of soil profiles around the globe. Soil attributes for each soil type are determined by the Soilprogram by sampling the WISE database. The program allows specification of the depth of each soil horizon for which attributes are to be determined. Soil attributes are aggregated from the 5-min resolution to coarser resolutions by taking an arithmetic average over all 5-min pixels in the model grid cell.

The remaining soil characteristics, such as porosity, saturated hydraulic conductivity, and the exponent for the unsaturated hydraulic conductivity equation were based on Cosby et al. (1984). The moisture contents at field capacity and wilting point were determined by calculating the moisture retention at a matric pressure of -33 kPa and -1500 kPa, respectively. The program from Gerakis (1999) was used to convert soil textural information to the United States Department of Agriculture soil textural classes used by Cosby et al. (1984).

The soil depth was somewhat arbitrarily chosen as 1 m for all grid cells, with an upper horizon of 0.3 m and a lower horizon of 0.7 m. In addition a deeper layer without roots was specified, from which base flow was generated using the ARNO base flow formulation [see section 3a(2)]. This layer had a water storage capacity of 100 mm, corresponding to a depth of about 0.25 m, depending on the porosity.

3) VEGETATION

Vegetation types were taken from the Advanced Very High Resolution Radiometer (AVHRR)-based, 1-km, global land classification from Hansen et al. (2000), which uses 13 land cover classes plus a water class. For this study, the bare ground class and the urban builtup class were combined, while the water class was not considered to be part of the land area, resulting in 12 unique vegetation classes. Vegetation fractions were determined as the area occupied by a vegetation type divided by the total land area in each $2^\circ \times 2^\circ$ grid cell. As in the case of the elevation bands, a threshold of 1% of the land area was used to limit the number of vegetation types per model grid cell.

Vegetation parameters such as height, and minimum stomatal resistance were assigned to each vegetation class based on a variety of sources. As in Nijssen et al. (1997), minimum stomatal resistance values were adapted from Sellers et al. (1994). Roughness lengths and displacement heights were calculated from assumed average vegetation heights following Calder (1993). Architectural resistances were taken from Ducoudré et al. (1993). The fraction of roots in the top two soil layers was assigned in such a way that trees would predominantly take moisture from the second soil horizon, while short vegetation such as grasses and crops would take most of their moisture from the upper soil horizon.

LAI values, used in the calculation of interception storage and evapotranspiration, were based on Myneni

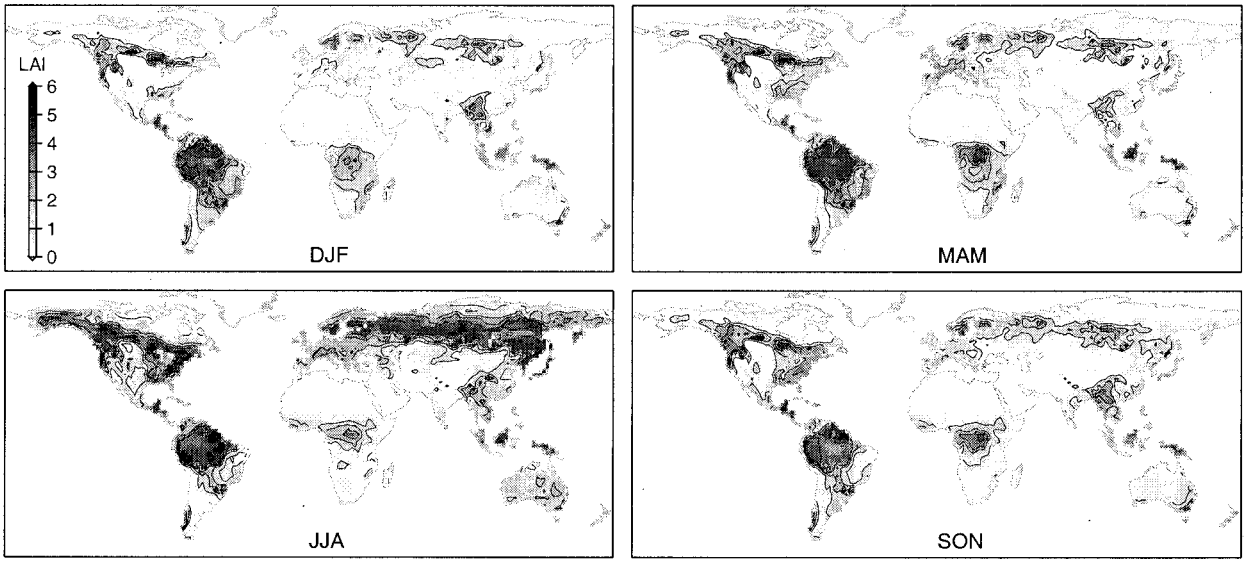

FIG. 4. Mean seasonal LAI. Contours correspond to the ticks on the shading bar. DJF is Dec, Jan, Feb; MAM is Mar, Apr, May; JJA is Jun, Jul, Aug; and SON is Sep, Oct, Nov.

et al. (1997), who produced a 15-min global LAI dataset by relating AVHRR-based normalized difference vegetation index values to LAI using a three-dimensional radiative model. The LAI values were allowed to vary by month, but were kept constant from year to year. The 15-min LAI data were mapped to the individual vegetation types using the following method. At the 15-min resolution, the dominant land cover types were calculated for the globe from the 1-km resolution land cover dataset. Those cells in which a single land cover dominated (arbitrarily defined as having in excess of 80% coverage) were identified, and the corresponding LAI values of Myneni et al. (1997) were assumed to be representative of the land cover at that cell location. The LAI values were then assigned to the VIC partial coverages on a cell-by-cell basis by averaging the dominant cell LAI values for the appropriate land cover type within a 2° window.

The resulting seasonal LAI patterns are shown in Fig. 4. LAI values are high in the humid Tropics and low in the desert and semiarid areas of low- and midlatitudes. High summer LAI values at high northern latitudes correspond to the location of the boreal forest and agricultural crops. The summer LAI values for the boreal forest range from 4 to 5 and are near the upper end of the range reported in the literature (Chen et al. 1997).

c. Model implementation

The simulation period was 1 January 1979–31 December 1993. The first year of the model simulations was used as a spinup period and was discarded to limit the effects of the initial conditions on the model simulations. Consequently the period of analysis was from 1 January 1980 to 31 December 1993. Initial soil moistures were set to 80% of the field capacity for each 2° × 2° grid cell.

d. Derived variables

Model-derived variables include evapotranspiration, runoff, soil moisture storage in the upper 1 m of the soil, snow water equivalent, and total terrestrial water storage. The latter term includes all water storage, including deeper soil layers, and canopy storage, in addition to the moisture stored in the upper 1 m of soil and the water stored as snow.

Comparison of soil moisture storage between different models and between models and observations is complicated because of differences in soil parameterizations employed by the various models. Koster and Milly (1997) have shown that different land surface schemes produce different evapotranspiration and runoff for the same soil moisture storage. They conclude that differences in evapotranspiration predictions among models can be explained in terms of the average transpiration efficiency across the active soil moisture range for a given model, and the fraction of this range over which runoff can be generated. Dirmeyer et al. (1999) found that simple normalization of the soil wetness using the wilting point and field capacity did not resolve the differences in mean soil moistures among the different schemes, and suggested that a method based on soil moisture changes might be more practical. However, soil moisture changes are not always easy to evaluate in terms of seasonal averages or in terms of wet and dry periods. Maurer et al. (2000) describe a method for normalizing soil moisture. The soil moisture series are normalized by subtracting the lowest soil moisture value during the period of interest. In effect, only the active

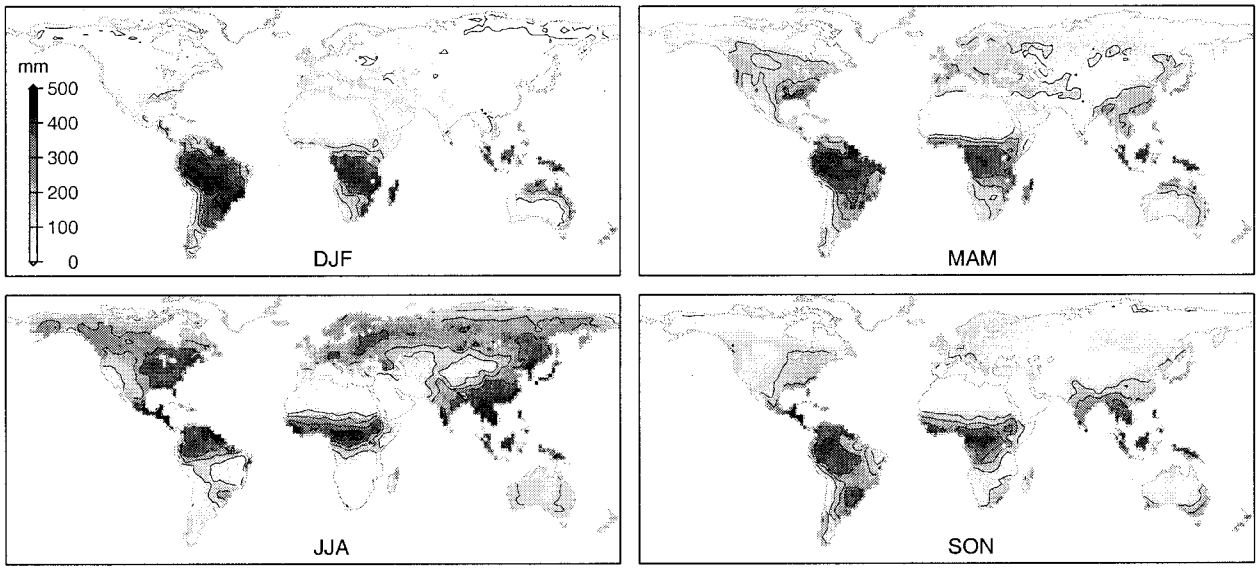

FIG. 5. Mean seasonal evapotranspiration (1980–93). Contours correspond to the ticks on the shading bar.

range of soil moistures remains. This approach removes to some extent differences due to different specifications of soil textural and hydraulic properties.

4. Discussion

The results can be discussed in terms of the water balance equation:

$$\frac{\Delta S}{\Delta t} = P - E - R, \tag{1}$$

where ΔS is the change in water storage over a given area during the time period Δt, P is the precipitation, E is the evapotranspiration, and R is runoff over the same area during the same period. Because the VIC model does not explicitly consider water stored in lakes or water stored as deep ground water, the total storage is the sum of soil moisture storage, groundwater storage, snow water equivalent, and canopy storage. Evapotranspiration in this case is the net sum of transpiration by plants, evaporation from canopy storage, evaporation from bare soil, sublimation from intercepted snow and from the snowpack, and condensation. Runoff is the sum of the fast response surface runoff and the slower drainage from the deepest soil layer.

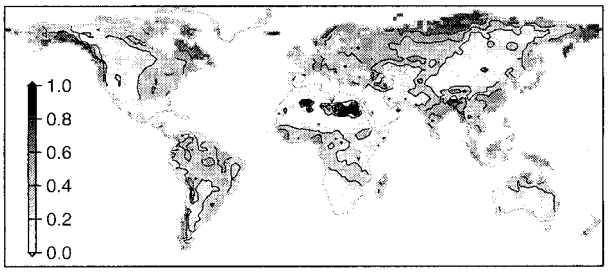

FIG. 6. Mean annual runoff ratio. Contours correspond to the ticks on the shading bar.

a. Global patterns

A survey of the results shows that mean seasonal evapotranspiration is high throughout the year in the humid Tropics, where both temperatures and rainfall amounts are high (Fig. 5). The highest mean seasonal evapotranspiration rates of about 6 mm day^{-1} occur in Southeast Asia during the monsoon season in June, July, and August, and in the central part of the Amazon basin during the months December, January, and February when precipitation in this area reaches its maximum. Seasonal evapotranspiration is also high in the Northern midlatitudes during the summer when the vegetation is fully developed (see Fig. 4), and in the boreal forest zone. The relatively high summer evapotranspiration in the boreal forest zone results partly from the high LAI values, which as discussed in section 3b(3) may be anomalous. Low evaporation rates occur in moisture-limited environments, such as the Sahara, Southern Africa, Central Asia, Australia, and the southwestern parts of North and South America, and in energy limited environments, such as the mid and high Northern latitudes during the Northern Hemisphere autumn, winter, and spring.

Figure 6 shows the simulated mean annual runoff ratio, defined as the fraction of the mean annual precipitation that is converted to runoff. Low runoff ratios occur in arid and semiarid areas, where most of the precipitation evaporates. The highest runoff ratios occur at those high northern latitudes where fall and winter precipitation is dominant. Most of this precipitation falls

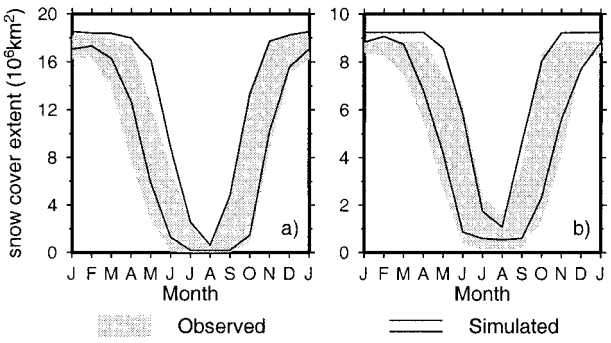

FIG. 7. Observed and simulated range in snow cover extent for (a) Eurasia and (b) North America [observations from National Snow and Ice Data Center (1978–95)].

in the form of snow, and becomes runoff during the spring and summer snowmelt season when soil moisture storage capacities are exceeded. The anomalously high runoff ratios for some cells in the eastern and central Sahara are a modeling artifact. Soil moisture was globally initialized to 80% of field capacity (section 3c), but precipitation in these areas is virtually nonexistent and vegetation is largely absent. In the VIC model, bare soil evaporation can occur only from the topsoil layer. Consequently, the initial moisture from the lower soil layer will slowly drain, resulting in very small runoff amounts over the 14-yr analysis period. Because precipitation amounts are even smaller, apparent annual runoff ratios are anomalously high.

Seasonal runoff ratios (not shown) are much larger than one at midnorthern latitudes during spring and at high northern latitudes during summer. Part of the runoff during this period originates as water stored in the snowpack and seasonal runoff ratios can therefore be greater than one. Because annual evapotranspiration at high northern latitudes is energy limited, the soils remain relatively wet throughout the year and little excess storage capacity is available to store the snowmelt in the soil. Another location with high runoff ratios is the northwestern coast of North America, where precipitation is high.

The model-predicted, monthly range in snow cover extent north of 50°N in Eurasia and North America for the period of 1980–93 was compared with snow cover extent estimates based on the digital National Oceanic and Atmospheric Administration–National Environmental Satellite Data Information Service (NOAA–NESDIS) Weekly Northern Hemisphere Snow Charts. Figure 7 shows for each month the range in snow cover extent in Eurasia and North America, both modeled and observed, for the 1980–93 period. The simulated snow-covered area was defined as the area of those grid cells that had a mean snow water equivalent greater than 10 mm during a given month. The 10-mm threshold was used to avoid confounding the results with small amounts of snow in high-elevation areas where the snow lingers until late in the summer. The range was calculated by finding the minimum and maximum snow cover extent during each month in the 14-yr period. The original NOAA–NESDIS weekly snow charts are derived from manual interpretation of AVHRR, Geostationary Operational Environmental Satellite, and other visible-band satellite data (National Snow and Ice Data Center 1996).

The monthly range in snow cover extents compared well for Eurasia (Fig. 7a), with maximum snow cover extents of about 18×10^6 km^2 during the winter and early spring and minimum snow cover extent in August. The range in snow cover extent is largest during the snow accumulation and snowmelt periods in fall and spring, and smallest near the end of the winter (February) and near the end of summer (August). The model-simulated range in snow extent is somewhat smaller than the observed range (as indicated by the shaded band in Fig. 7a). This tendency is more pronounced in the model-simulated snow cover extent over North America (Fig. 7b). Again, the observed and simulated maximum snow cover extent are both around 9×10^6 km^2, with model-simulated snow extents slightly larger. Minimum snow cover extent occurs in August, but the observed snow cover extent shows larger variations. The model also shows that some of the snow at the highest elevations never disappears, resulting in a permanent snow cover over an area of about 0.5×10^6 km^2. The greater difference in the observed and simulated range of snow cover extent in North America may partly result from the greater variation of topography in northern North America than in Eurasia.

Figure 8 shows simulated mean seasonal soil moisture storage in the upper 1 m of the soil. The arid and semiarid regions show low soil moisture storage in all four seasons. High soil moisture values are apparent in the humid Tropics, where high precipitation amounts keep the soil near or above field capacity during most seasons; in Europe and the eastern United States during the winter and spring, when low temperatures limit the amount of evapotranspiration; in Southeast Asia during the monsoon season in summer and fall; and at mid and high northern latitudes following snowmelt.

The relationship between soil moisture storage and snowmelt is made more obvious by comparing mean seasonal soil moisture (Fig. 8) with mean seasonal snow water equivalent (Fig. 9). High soil moisture contents in Siberia during the summer months are largely due to snowmelt in the late spring.

Relatively large changes in seasonal soil moisture are apparent in the midlatitudes, where higher summer temperatures lead to increased evapotranspiration. This is particularly apparent in regions such as the Mediterranean and the northern Pacific Coast of North America, where the precipitation is winter dominant. Tropical and subtropical regions that display relatively large changes in soil moisture are the Indian subcontinent and southeast Asia, the southern boundary of the Amazon basin in South America, and the east coast of Africa. In all

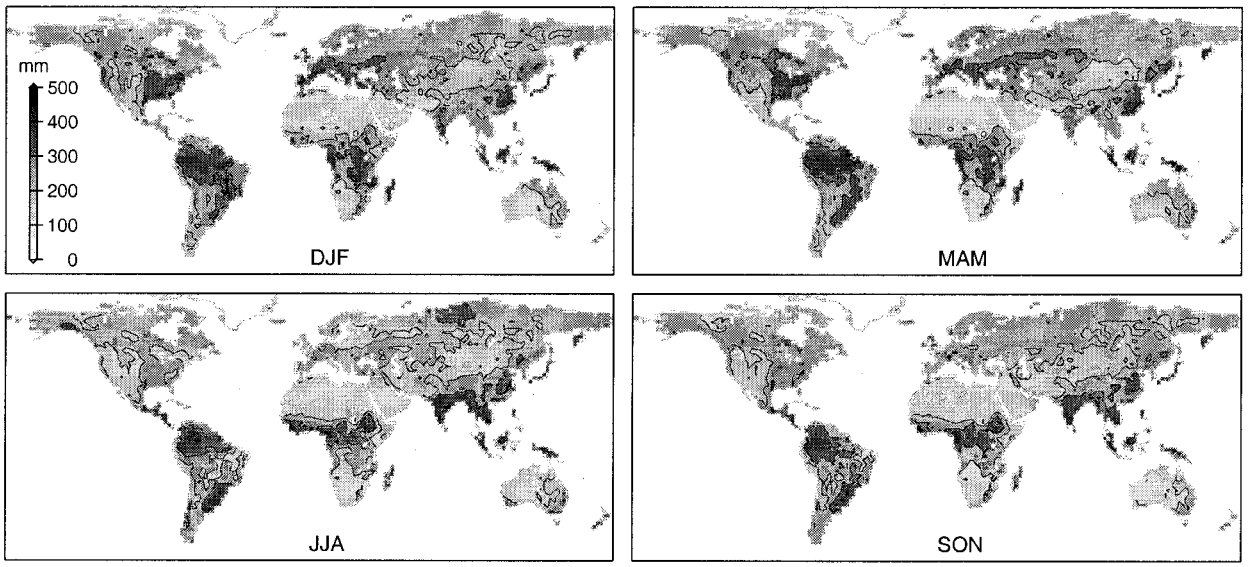

FIG. 8. Simulated seasonal soil moisture storage for the upper 1 m of soil during the period of 1980–93. Contours correspond to the ticks on the shading bar.

these areas precipitation shows a strong seasonality with distinct dry and wet seasons.

b. Continental water balance

Estimates of the mean annual water balance components for the globe and the continents (except Greenland and Antarctica) are summarized for this study and various previous studies in Table 1. If the averaging period is long enough, mean storage change will be close to zero, and the difference between precipitation and evaporation (or evapotranspiration) should equal runoff. The model simulations are consistent in this respect. Because the averaging period differs among the studies in Table 1, and because the boundary between Europe and Asia may differ somewhat, some variation in the results is to be expected. For all land areas combined and for most individual continents, the independent estimates for P and E agree relatively well, although differences between the estimates can be large for individual continents. For example, precipitation estimates for South America range from 1440 to 1648 mm (1449 mm in this study). Because the evaporation estimates for South America vary much less, the largest relative difference is in the runoff estimates, which range from 415 to 678 mm (454 mm in this study).

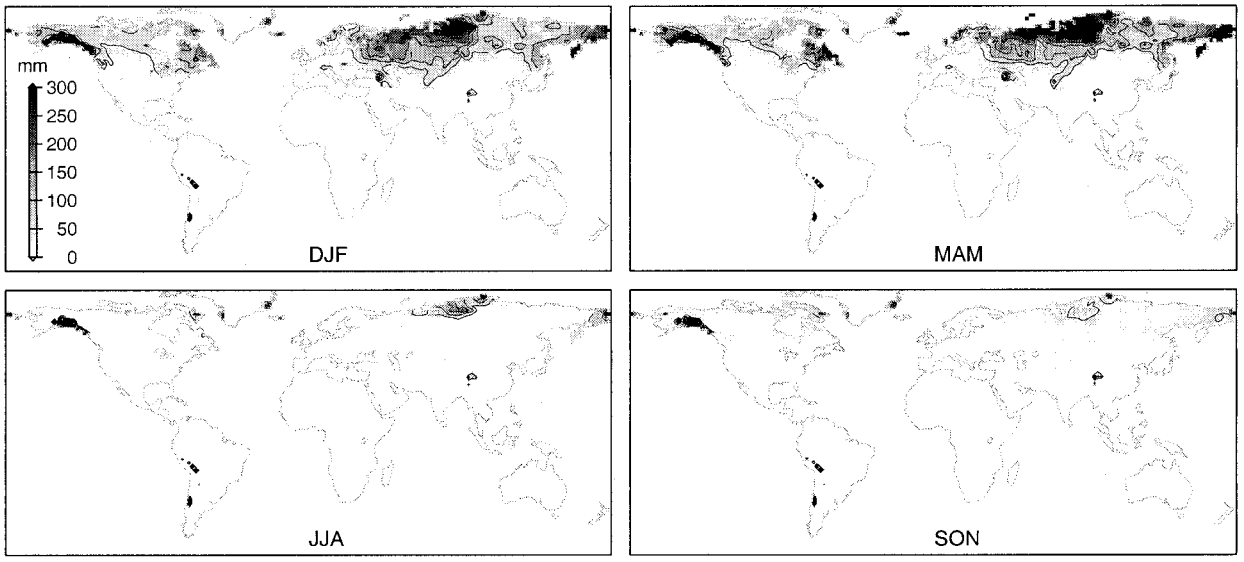

FIG. 9. Simulated mean seasonal snow water equivalent. Contours correspond to the ticks on the shading bar.

TABLE 1. Annual continental water balance (mm yr^{-1}). Continents are defined according to Oki et al. (1995). Europe includes Turkey and extends as far east as the Urals. Australia includes New Zealand and New Guinea. All estimates except for Oki et al. (1995) and Oki (1999) are based on hydrological methods. The estimate from Oki et al. (1995) and Oki (1999) are based on atmospheric water balance computations using global analysis data from ECMWF for the period of 1985–88 and 1989–92, respectively.

Variable	All lands	Asia	Europe	Africa	North America	South America	Australia	Reference
P	727	590	769	655	633	1449	680	
E	483	366	436	511	409	995	485	This study
R	244	224	333	145	222	454	193	
P	834	726	734	686	670	1648	736	
E	540	433	415	547	383	1065	510	Lvovitch (1973)
R	294	293	319	139	287	583	226	
P		515	593	728	738	1440	495*	
E		346	328	525	423	990	418*	Kalinin (1968)
R		169	265	203	315	450	77*	
P	746	696	657	696	645	1564	803/447**	
E	480	420	375	582	403	946	534/420**	Baumgartner and Reichel (1975)
R	266	276	282	114	242	618	269/27**	
$P - E = R$	303	300	273	153	315	678	278	Korzun (1978)
$P - E = R$	165	235	136	−100	263	415	54	Oki et al. (1995)
$P - E = R$	244	244	197	4	318	773	24	Oki (1999)

* The definition of Australia used by Kalinin (1968) does not include New Zealand or New Guinea.

** The first value includes the islands in Oceania and much of the Pacific Ocean; the second value refers to the mainland of Australia only.

Estimated precipitation over Europe is higher in this study than in any of the other estimates. Consequently, this study also reports the highest evapotranspiration and runoff estimates for Europe. However, the partitioning of precipitation into evapotranspiration and runoff is almost identical for the four estimates for which both precipitation and evapotranspiration are available, with the runoff ratio ranging from 0.43 to 0.45 (0.43 in this study) and the evapotranspiration ratio ranging from 0.55 to 0.57 (0.57 in this study). On a global scale the runoff ratio varies from 0.34 (this study) to 0.36 for the three available estimates.

Figure 10 shows the mean monthly water balance terms for each of the continents. Asia, North America, and Europe all show a strong evapotranspiration peak during June, July, and August, when temperatures are highest. All three continents show an increase in runoff and soil moisture storage that coincides with a rapid decrease in snow water equivalent. The change in snow water equivalent and increase in runoff is most pronounced in Europe. Soil moisture storage in Europe and North America declines during the summer months, when evapotranspiration rates are high, and is restored during the fall months.

In the Southern Hemisphere, the changes in evapotranspiration and soil moisture storage are more closely linked to the seasonality of precipitation, because snow processes do not play a large role. The continental average fluxes and storage changes do not show a distinct seasonality for Africa, which straddles the equator, covers a large range of climatic zones, and where snow processes do not play a role in the water balance.

One of the contributions of this study is a daily model forcing dataset spanning a 15-yr period, compared with the 2-yr period used in pilot phase of the GSWP (Dirmeyer et al. 1999). Figure 11 shows the simulated, monthly range in mean soil moisture storage in the upper 1 m of soil for each continent for the period 1980–93. The simulated monthly range of the same quantity over the period 1987–88 is superimposed. The ranges were determined by calculating the average soil moisture storage over each continent and locating the minimum and maximum soil moisture storage value for each month during the period of interest. The figure stresses the importance of extending the time series of soil moisture storage values for a sufficiently long period in order to characterize the variability and range of soil moisture values that can be expected. This was also shown by Schlosser et al. (1997, 2000). This is not meant to imply that the period 1980–93 is long enough for climatological studies, on the contrary, it emphasizes the need for soil moisture simulations covering even longer time periods. In most cases the monthly range in soil moisture values during the 1987–88 period was much less than half the range of modeled soil moisture values during the longer 1980–93 period.

c. Soil moisture storage

1) COMPARISON WITH MINTZ AND SERAFINI (1992)

The climatology of monthly soil moisture values produced by Mintz and Serafini (1992) is widely used in the climate and weather modeling community. One of the shortcomings of this dataset is that snow accumulation is not accounted for (Matsuyama and Masuda 1997). Figure 12 shows the soil moisture storage in the upper 1 m of the soil for January, April, July, and October as a fraction of field capacity [cf. Fig. 10 in Mintz and Serafini (1992)]. Direct comparison of the two soil

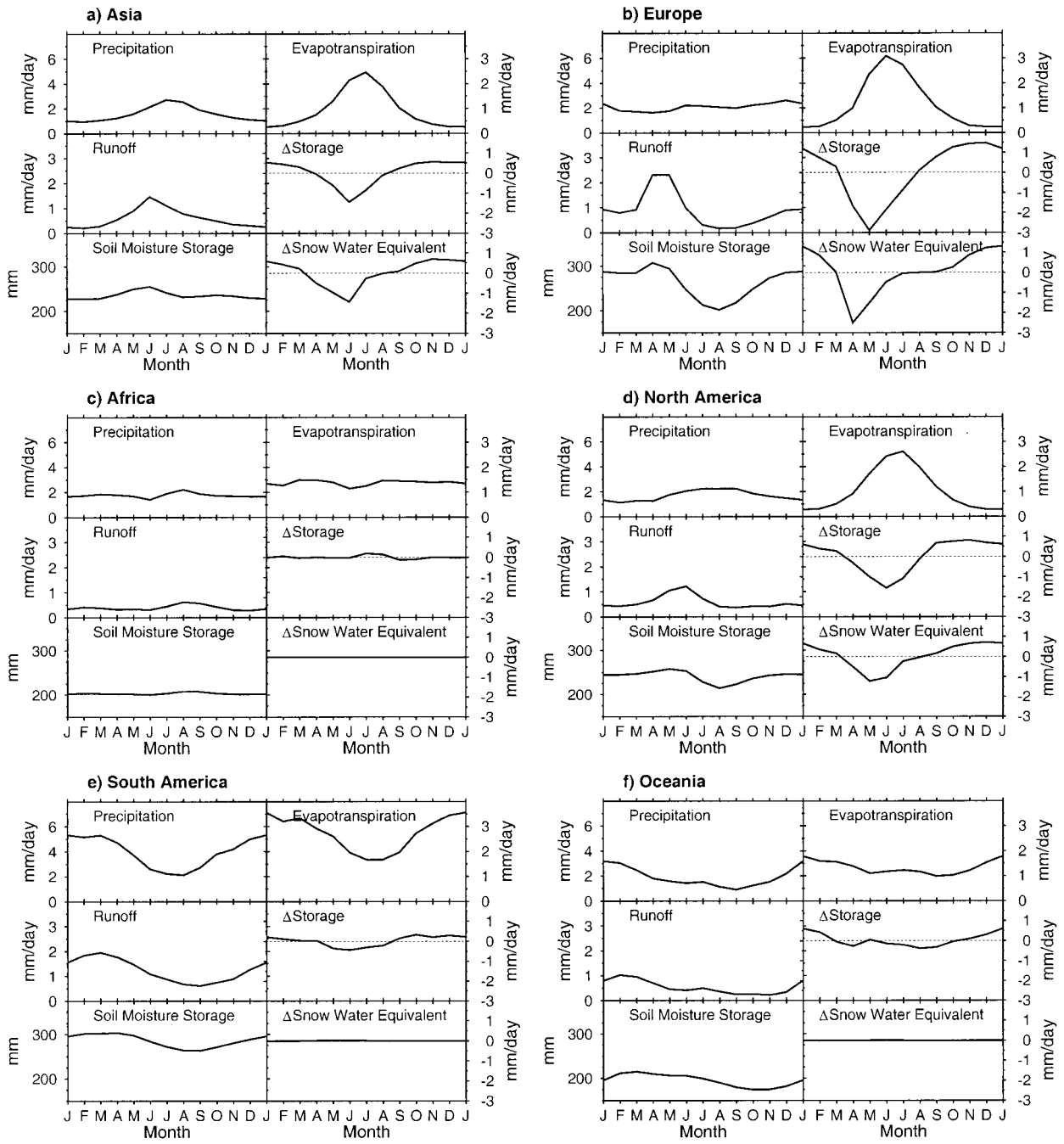

FIG. 10. Mean monthly continental water balance component: (a) Asia, (b) Europe, (c) Africa, (d) North America, (e) South America, and (f) Australia (including New Zealand and New Guinea).

moisture fields is difficult, because different runoff generation mechanisms were used, and the soil moisture reservoir sizes were different. Mintz and Serafini (1992) defined their soil moisture storage in terms of the differences between field capacity and wilting point, with the minimum moisture storage at wilting point and the maximum moisture storage at field capacity. Maximum allowed storage was 150 mm. Runoff was generated using a bucket model (Budyko 1956; Manabe 1969). In contrast, soil moisture in the VIC model can fall below wilting point through evaporation from the bare soil and more importantly through drainage. Runoff is generated over the entire range of soil moisture values. Maximum soil moisture in the VIC model is equal to the porosity of the soil, and soil moisture can stay above field capacity in areas where precipitation and snowmelt exceed

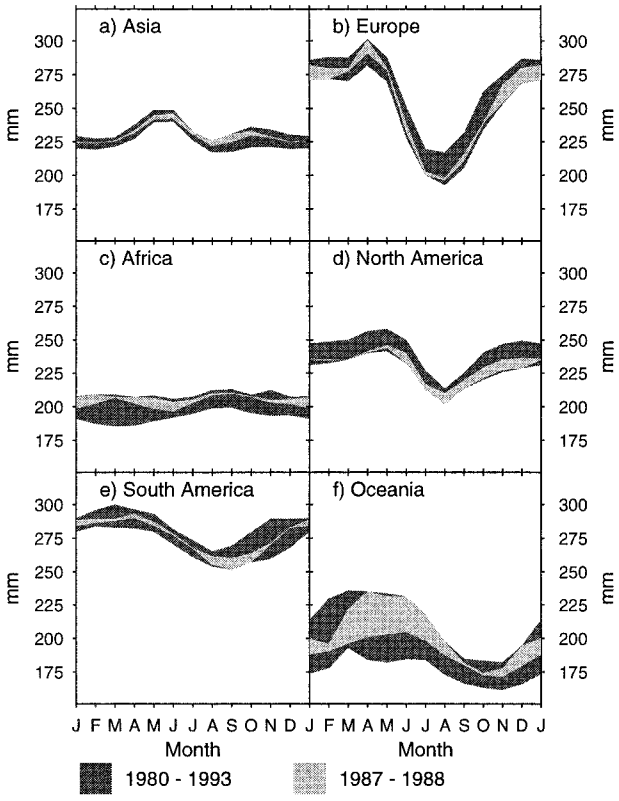

FIG. 11. Monthly range in soil moisture storage for the period of 1980–93 for each continent. Also shown are the soil moisture storage ranges for the period of 1987–88, corresponding to the years covered by the GSWP.

the sum of drainage and evaporation. Consequently, soil moisture storage expressed as a fraction of field capacity varies between zero and one in Mintz and Serafini (1992), but can be greater than one in this study. In addition, a value of zero would indicate that no water remained in the soil. Because of these differences, we limit ourselves here to a comparison of the soil moisture patterns from the two studies rather than the absolute storage values.

Generally, the patterns of soil moisture storage in this study mirror those of Mintz and Serafini (1992), with high soil moistures in the humid Tropics during most of the year, and at mid to high northern latitudes in January and April. The main difference is that in this study, soils at the highest latitudes remain very wet till late in the summer, because of snowmelt in late spring. Because of the absence of snow processes in Mintz and Serafini (1992), the soils at high latitudes begin to dry in spring as soon as the temperatures increase enough for evapotranspiration to exceed precipitation.

2) COMPARISON WITH OBSERVATIONS

A number of existing observational datasets have been assembled as part of the Global Soil Moisture Data Bank (Robock et al. 2000). We compared our results with two of these datasets, one for Illinois (Hollinger and Isard 1994), and one for central Eurasia (Vinnikov and Yeserpova 1991). The method of Maurer et al. (2000) discussed in section 3d was used to normalize both the observations and simulations.

The Illinois dataset consists of 19 grass-covered sites in Illinois, where soil moisture measurements were obtained by neutron-probe during the period of 1981–96. Figure 13 shows the normalized mean annual soil mois-

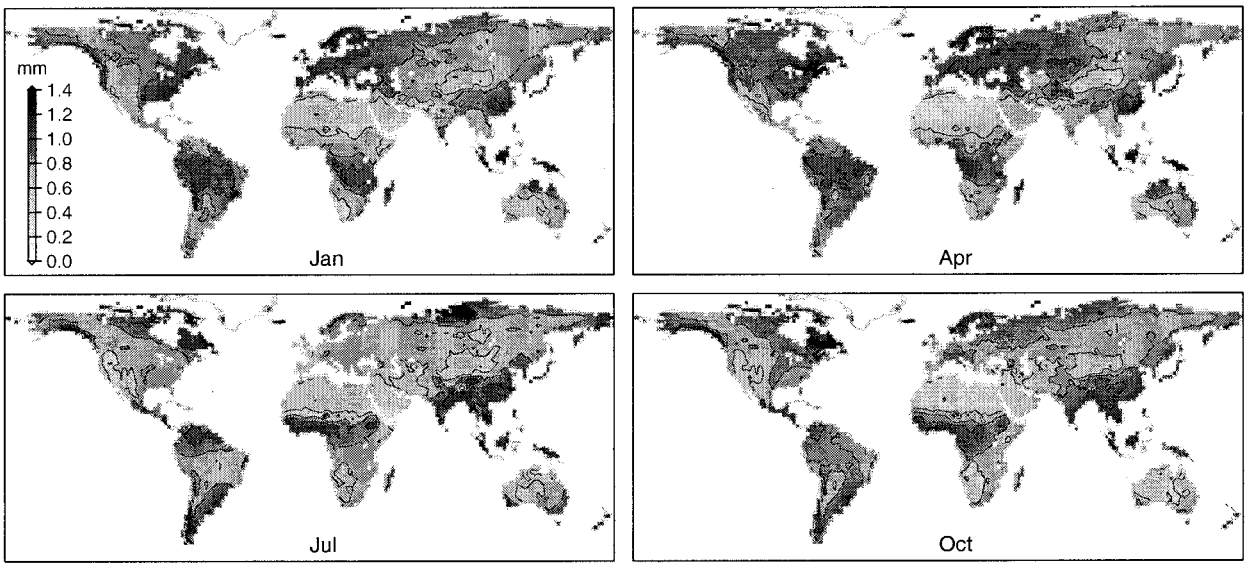

FIG. 12. Mean monthly soil moisture storage in tenths of field capacity for (a) Jan, (b) Apr, (c) Jul, and (d) Oct. Contours correspond to the ticks on the shading bar.

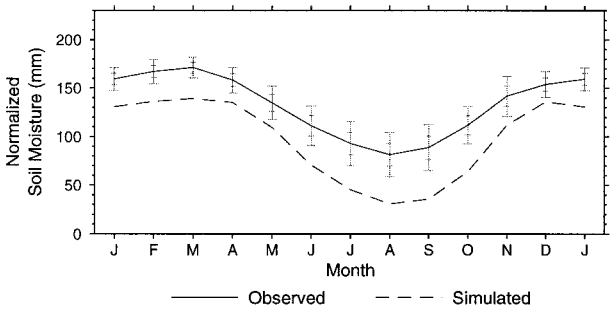

FIG. 13. Normalized observed and simulated annual cycle of soil moisture storage in the upper 1 m of soil in Illinois for the period of 1981–92 [observations from Hollinger and Isard (1994); see also Robock et al. (2000)]. The error bars show the 95% confidence interval (outer tick) and one standard deviation (inner tick) of the observed means.

ture cycle. Error bars that show the 95% confidence interval and one standard deviation of the estimate of the mean are superimposed on the observations. The effect of between-site covariances was not included. Because the covariances between the stations are likely to be positive, the estimated variance is conservative. The normalized mean monthly simulated soil moisture cycle represents the average of six model grid cells. The change in soil moisture is generally well predicted, although the simulated flux is greater than observed in June, when more moisture than observed leaves the soil through runoff and evapotranspiration, and again in autumn when more water than observed enters the soil column. Consequently, the difference between observed and simulated soil moisture is greater during the summer than during the winter months.

Despite normalizing both the observed and simulated soil moisture time series, the normalized simulated soil moisture still shows a considerable low bias. Examination of the normalized monthly time series for the period of 1980–93 (not shown) shows that the observations exhibit a greater interannual persistence than the simulations. That is, years with high soil moisture during the summer months tend to follow each other. As suggested by one of the reviewers of this paper, a major factor in this overall dryness is likely to be the uniform, shallow soil depth prescribed in our model. The observed data are all for the top 1 m of a deeper, active soil column, so that upward diffusion from deeper layers can replenish shallow soil moisture. Another likely source of error, although less important, is that the model grid cells are covered by a mixture of vegetation types, whereas the observation stations were all located in grassland areas.

The Eurasian soil moisture dataset consists of observations of plant-available soil moisture at 130 grassland sites in central Eurasia for the period of 1978–85 (Robock et al. 1998; Vinnikov and Yeserpova 1991; Vinnikov et al. 1996). Comparisons with model simulations were made for the 6-yr period 1980–85, and used only stations with observations for at least 66 out of 72 months. Both observations and simulations were normalized using the procedure described above. Mean annual normalized soil moisture cycles were calculated for eight regions along a roughly west–east transect (Fig. 14). Because the Eurasian dataset covers a shorter time period and contains fewer stations per region than in the Illinois case, the related error bars are larger.

Both model results and observations show a decrease in the amplitude of the annual cycle from west to east, corresponding to a transition from wetter to drier regions. In all regions observed and simulated soil moisture reach a maximum in spring and a minimum in mid to late summer. As in Illinois, the mean simulated summer minima exhibit a low bias, particularly in regions A and B. Again, the shallow soils in the simulation are a likely source of error, because much of mid- and high-latitude Eurasia has shallow water tables that interact with the surface layers.

5. Conclusions

The daily model forcing dataset for global land areas for the period of 1979–93 is suitable for application with most land surface parameterizations. Daily precipitation and temperature are based on station observations and scaled to monthly mean time series developed by other researchers (Huffman et al. 1997; Hulme 1995; Jones 1994). Daily wind speeds are based on reanalysis data (Kalnay et al. 1996) and the remaining meteorological variables are derived from the precipitation and temperature series (Kimball et al. 1997; Thornton and Running 1999). The advantages of the dataset described here are the high temporal resolution (daily), the long time period (15 yr) and its global cover. The dataset facilitates global simulations and evaluation of land surface parameterizations without relying heavily on GCM output, which generally exhibits too large a bias for direct application in hydrological models (Leung et al. 1999).

Application of this forcing dataset to the VIC model resulted in a set of derived variables, consisting of snow water equivalent, evapotranspiration, runoff, and soil moisture storage. The monthly range in simulated snow cover extent compared well with the NOAA–NESDIS Weekly Northern Hemisphere Snow Charts (National Snow and Ice Data Center 1996), especially in Eurasia. The simulated interannual variability in snow cover extent in North America was somewhat underpredicted. The components of the global and continental water balance were similar to those from previous estimates, although runoff is somewhat lower for some continents. Patterns of simulated soil moisture storage are similar to those of Mintz and Serafini (1992), but use of a more sophisticated hydrology model leads to a larger range in soil moisture contents. Also, snow processes were not accounted for in the monthly climatology of Mintz and Serafini (1992). Comparison of interannual soil

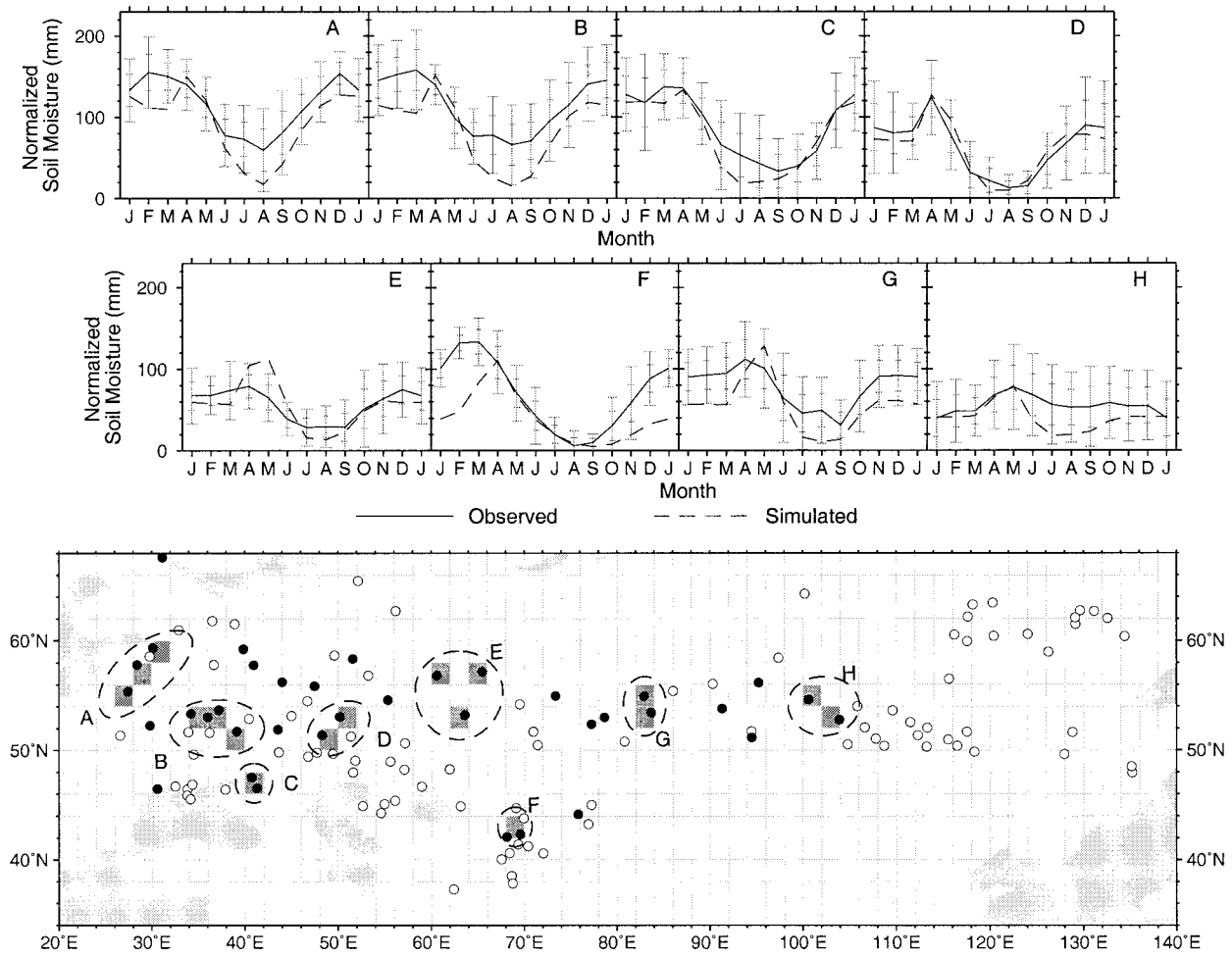

FIG. 14. Normalized observed and simulated soil moisture along a transect in central Eurasia for the period of 1980–85 [observations from Vinnikov and Yeserpova (1991); see also Robock et al. (2000)]. The bottom figure shows all 130 grassland stations at which soil moisture was collected (○ and ●). The closed circles (●) are the stations with the most complete records (reporting during at least 60% of the winter months of Dec–Mar). The dark gray squares are the model grid cells used in the comparison. Within each of the dashed ellipses, the observed and the simulated values were averaged and plotted in the eight top figures. The top figures show the mean monthly observed and simulated soil moisture. The error bars show the 95% confidence interval (outer tick) and one standard deviation (inner tick) of the observed means.

moisture variability for the entire analysis period (1980–93) with the analysis period of the pilot phase of the GSWP (1987–88; Dirmeyer et al. 1999) stresses the importance of using a relatively long time series in order to capture this variability. The interannual variability during the 2-yr period is for most continents less than half of that during the longer period used here. Comparison with observations reveals that the annual cycle and spatial patterns in soil moisture are well captured, both in Illinois and in central Eurasia, but modeled soil moisture is lower than observed and shows less interannual persistence than the observations. One likely explanation is that the interaction between the prescribed, shallow (1 m) soils with deeper soil layers is not represented in the VIC model. A mechanism for upward diffusion of soil moisture and perhaps eventual coupling with a regional groundwater model are suggested as solutions.

The complete forcing dataset for the period of 1979–93, as well as the derived variables for the analysis period of 1980–93, are available for use in other studies. At the time of writing, the data could be accessed on the Internet at http://www.hydro.washington.edu/Lettenmaier/DataInfo.html.

Acknowledgments. We are grateful to Greg M. O'Donnell for his help with the simulations and graphics. This work was supported by the U.S. Environmental Protection Agency under Grant R 824802-01-0 to the University of Washington. Retrieval of the daily temperature and precipitation station observations from the NCAR archives was supported by NCAR under Grant

35371107. The second author's work was supported by a fellowship in the NOAA Postdoctoral Program in Climate and Global Change.

REFERENCES

Abdulla, F. A., D. P. Lettenmaier, E. F. Wood, and J. A. Smith, 1996: Application of a macroscale hydrologic model to estimate the water balance of the Arkansas–Red River Basin. *J. Geophys. Res.,* **101,** 7449–7459.

Batjes, N. H., 1995: A homogenized soil data file for global environmental research: A subset of FAO, ISRIC and NCRS profiles. Rep. 95/10, International Soil Reference and Information Centre, Wageningen, Netherlands, 50 pp. [Available from ISRIC, P.O. Box 535, 6700 AJ Wageningen, Netherlands.]

Baumgartner, A., and E. Reichel, 1975: *The World Water Balance: Mean Annual Global, Continental and Maritime Precipitation, Evaporation and Runoff.* Elsevier Scientific, 179 pp.

Betts, A. K., J. H. Ball, A. C. M. Beljaars, M. J. Miller, and P. A. Viterbo, 1996: The land surface–atmosphere interaction: A review based on observational and global modeling perspectives. *J. Geophys. Res.,* **101,** 7209–7225.

Bras, R. A., 1990: *Hydrology, an Introduction to Hydrologic Science.* Addison-Wesley, 643 pp.

Bristow, K. L., and G. S. Campbell, 1984: On the relationship between incoming solar radiation and daily maximum and minimum temperature. *Agric. For. Meteor.,* **31,** 159–166.

Budyko, M., 1956: *Heat Balance of the Earth's Surface* (in Russian). Gidrometeoizdat, 255 pp.

Calder, I. R., 1993: Hydrologic effects of land-use change. *Handbook of Hydrology,* D. R. Maidment, Ed., McGraw-Hill, 13.1–13.50.

Campbell, G. S., 1974: A simple method for determining unsaturated conductivity from moisture retention data. *Soil Sci. Soc. Amer. J.,* **117,** 311–314.

Carter, A. J., and R. J. Scholes, 1999: Generating a global database of soil properties. Environmentek CSIR, 10 pp.

Chen, J. M., P. D. Blanken, T. A. Black, M. Guilbeault, and S. Chen, 1997: Radiation regime and canopy architecture in a boreal aspen forest. *Agric. For. Meteor.,* **86,** 107–125.

Cosby, B. J., G. M. Hornberger, R. B. Clapp, and T. R. Ginn, 1984: A statistical exploration of the relationships of soil moisture characteristics to the physical properties of soils. *Water Resour. Res.,* **20,** 682–690.

Dingman, S. L., 1994: *Physical Hydrology.* Prentice-Hall, 575 pp.

Dirmeyer, P. A., 1995: Problems in initializing soil wetness. *Bull. Amer. Meteor. Soc.,* **76,** 2234–2240.

——, A. J. Dolman, and N. Sato, 1999: The pilot phase of the Global Soil Wetness Project. *Bull. Amer. Meteor. Soc.,* **80,** 851–878.

Ducoudré, N. I., K. Laval, and A. Perrier, 1993: SECHIBA, a new set of parameterizations of the hydrologic exchanges at the land–atmosphere interface within the LMD atmospheric general circulation model. *J. Climate,* **6,** 248–273.

Entin, J., A. Robock, K. Y. Vinnikov, S. Qiu, V. Zabelin, S. Liu, A. Namkhai, and T. Adyasuren, 1999: Evaluation of Global Soil Wetness Project soil moisture simulations. *J. Meteor. Soc. Japan,* **77,** 183–198.

Fan, Y., E. E. Wood, M. L. Baeck, and J. A. Smith, 1996: Fractional coverage of rainfall over a grid: Analyses of NEXRAD data over the southern plains. *Water Resour. Res.,* **32,** 2787–2802.

FAO, 1995: *The Digital Soil Map of the World, Version 3.5.* United Nations Food and Agriculture Organization, CD-ROM. [Available from Food and Agriculture Organization of the United Nations, Viale delle Terme di Caracalla, 00100 Rome, Italy.]

Geng, S., F. W. T. Penning, and I. Supit, 1986: A simple method for generating daily rainfall data. *Agric. For. Meteor.,* **36,** 363–376.

Gerakis, A., 1999: A computer program for soil textural classification. *Soil Sci. Soc. Amer. J.,* **63,** 807–808.

Goulden, M. L., B. Daube, S. Fan, D. Sutton, A. Bazzaz, J. W. Munger, and S. Wofsy, 1997: Physiological responses of a black spruce forest to weather. *J. Geophys. Res.,* **102,** 28 987–28 996.

Goutorbe, J. P., and Coauthors, 1997: An overview of HAPEX-Sahel: A study in climate and desertification. *J. Hydrol.,* **189,** 4–17.

Graham, S. T., J. S. Famiglietti, and D. R. Maidment, 1999: 5-minute, ½°, and 1° data sets of continental watersheds and river networks for use in regional and global hydrologic and climate system modeling studies. *Water Resour. Res.,* **35,** 583–587.

Hansen, M. C., R. S. DeFries, J. R. G. Townshend, and R. Sohlberg, 2000: Global land cover classification at 1 km spatial resolution using a classification tree approach. *Int. J. Remote Sens.,* **21,** 1331–1364.

Henderson-Sellers, A., Z.-L. Yang, and R. Dickinson, 1993: The Project for Intercomparison of Land-Surface Parameterization Schemes. *Bull. Amer. Meteor. Soc.,* **74,** 1335–1349.

——, A. J. Pitman, P. K. Love, P. Irranejad, and T. H. Chen, 1995: The Project for Intercomparison of Land Surface Parameterization Schemes (PILPS): Phases 2 and 3. *Bull. Amer. Meteor. Soc.,* **76,** 489–503.

Hollinger, S. E., and S. A. Isard, 1994: A soil moisture climatology of Illinois. *J. Climate,* **7,** 822–833.

Huffman, G. J., and Coauthors, 1997: The Global Precipitation Climatology Project (GPCP) Combined Precipitation Dataset. *Bull. Amer. Meteor. Soc.,* **78,** 5–20.

Hulme, M., 1995: Estimating global changes in precipitation. *Weather,* **50,** 34–42.

Jones, P. D., 1994: Hemispheric surface air temperature variations: A reanalysis and an update to 1993. *J. Climate,* **7,** 1794–1802.

Kalinin, G. P., 1968: *Problemy Global'noi Gidrologii* (Global Hydrology). Gidrometeorologicheskoe Izdatel'svo.

Kalnay, E., and Coauthors, 1996: The NCEP/NCAR 40-Year Reanalysis Project. *Bull. Amer. Meteor. Soc.,* **77,** 437–471.

Kane, D. L., R. E. Gieck Jr., L. D. Hinzman, and E. K. Lilly, 1997: Meteorologic and hydrologic data sets for the North Slope of Alaska along the Kuparuk River Watershed, 1985–1995. Internal Rep., Water Research Center, Institute of Northern Engineering, University of Alaska, Fairbanks, AK. [Available from Water Research Center Institute of Northern Engineering, University of Alaska, Fairbanks, Fairbanks, AK 99775-5860.]

Kimball, J. S., S. W. Running, and R. R. Nemani, 1997: An improved method for estimating surface humidity from daily minimum temperature. *Agric. For. Meteor.,* **85,** 87–98.

Korzun, V. I., Ed., 1978: *World Water Balance and Water Resources of the Earth.* Studies and Reports in Hydrology, Vol. 25, UNESCO, 663 pp.

Koster, R. D., and M. J. Suarez, 1995: The relative contributions of land and ocean processes to precipitation variability. *J. Geophys. Res.,* **100,** 13 775–13 790.

——, and P. C. D. Milly, 1997: The interplay between transpiration and runoff formulations in land surface schemes used with atmospheric models. *J. Climate,* **10,** 1578–1591.

——, M. J. Suarez, and M. Heiser, 2000: Variance and predictability of precipitation at seasonal-to-interannual timescales. *J. Hydrometeor.,* **1,** 26–46.

Legates, D. R., and C. J. Willmott, 1990: Mean seasonal and spatial variability in gauge-corrected, global precipitation. *Int. J. Climatol.,* **10,** 111–127.

Leung, L. R., A. F. Hamlet, D. P. Lettenmaier, and A. Kumar, 1999: Simulations of the ENSO hydroclimate signals in the Pacific Northwest Columbia River Basin. *Bull. Amer. Meteor. Soc.,* **80,** 2313–2329.

Levis, S., M. Coe, and J. Foley, 1996: Hydrologic budget of a land surface model: A global application. *J. Geophys. Res.,* **101,** 16 921–16 930.

Liang, X., D. P. Lettenmaier, E. F. Wood, and S. J. Burges, 1994: A simple hydrologically based model of land surface water and energy fluxes for general circulation models. *J. Geophys. Res.,* **99,** 14 415–14 428.

——, ——, and ——, 1996: One-dimensional statistical dynamic representation of subgrid spatial variability of precipitation in

the two-layer variable infiltration capacity model. *J. Geophys. Res.*, **101,** 21 403–21 422.

——, and Coauthors, 1998: The Project for Intercomparison of Land-surface Parameterization Schemes (PILPS) Phase 2(c) Red–Arkansas River Basin experiment: 2. Spatial and temporal analysis of energy fluxes. *Global Planet. Change,* **19,** 137–159.

Liston, G. E., Y. C. Sud, and G. K. Walker, 1993: Design of a global soil moisture initialization procedure for the Simple Biosphere model. NASA Tech. Memo. 104590, National Aeronautics and Space Administration, Greenbelt, MD, 138 pp.

Lohmann, D., R. Nolte-Holube, and E. Raschke, 1996: A large-scale horizontal routing model to be coupled to land surface parametrization schemes. *Tellus,* **48A,** 708–721.

——, and Coauthors, 1998a: The Project for Intercomparison of Land-surface Parameterization Schemes (PILPS) Phase 2(c) Red–Arkansas River Basin experiment: 3. Spatial and temporal analysis of water fluxes. *Global Planet. Change,* **20,** 161–179.

——, E. Raschke, B. Nijssen, and D. P. Lettenmaier, 1998b: Regional scale hydrology: I. Formulation of the VIC-2L model coupled to a routing model. *Hydrol. Sci. J.,* **43,** 131–141.

——, ——, ——, and ——, 1998c: Regional scale hydrology: II. Application of the VIC-2L model to the Weser River, Germany. *Hydrol. Sci. J.,* **43,** 143–158.

Lvovitch, M. I., 1973: The global water balance. *Eos, Trans. Amer. Geophys. Union,* **54,** 28–42.

Manabe, S., 1969: Climate and the ocean circulation. I. The atmospheric circulation and the hydrology of the earth's surface. *Mon. Wea. Rev.,* **97,** 739–774.

Matsuyama, H., and K. Masuda, 1997: Estimates of continental-scale soil wetness and comparison with the soil moisture data of Mintz and Serafini. *Climate Dyn.,* **13,** 681–689.

Maurer, E. P., G. M. O'Donnell, D. P. Lettenmaier, and J. O. Roads, 2000: Evaluation of NCEP–NCAR reanalysis water and energy budgets using macroscale hydrological simulations as a benchmark. *Observations and Modeling of the Land Surface Hydrological Processes,* V. Lakshmi, J. Albertson, and J. Schaake, Eds., Amer. Geophys. Union, in press.

Meeson, B. W., F. E. Corprew, J. M. P. McManus, D. M. Myers, J. Closs, K. Sun, D. Sunday, and P. Sellers, 1995: *ISLSCP Initiative—Global Data Sets for Land–Atmosphere Models, 1987–1988.* Vols. 1–5. NASA, CD-ROM. [Available from Goddard DAAC Help Desk, Code 902.2, NASA Goddard Space Flight Center, Greenbelt, MD 20771.]

Mintz, Y., 1984: The sensitivity of numerically simulated climates to land-surface boundary conditions. *The Global Climate,* J. J. Houghton, Ed., Cambridge University Press, 79–105.

——, and Y. V. Serafini, 1992: A global monthly climatology of soil moisture and water balance. *Climate Dyn.,* **8,** 13–27.

Montény, B. A., and Coauthors, 1997: The role of the Sahelian biosphere on the water and the CO_2 cycle during the HAPEX-Sahel experiment. *J. Hydrol.,* **188–189,** 516–535.

Myneni, R. B., R. R. Nemani, and S. W. Running, 1997: Estimation of global leaf area index and absorbed PAR using radiative transfer models. *IEEE Trans. Geosci. Remote Sens.,* **35,** 1380–1393.

National Snow and Ice Data Center, 1996: Northern Hemisphere EASE-Grid weekly snow cover and sea ice extent. Vols.1.0–2.0. EOSDIS NSIDC.

Nicks, A. D., and J. F. Harp, 1980: Stochastic generation of temperature and solar radiation data. *J. Hydrol.,* **48,** 1–17.

Nijssen, B., D. P. Lettenmaier, X. Liang, S. W. Wetzel, and E. F. Wood, 1997: Streamflow simulation for continental-scale river basins. *Water Resour. Res.,* **33,** 711–724.

Oki, T., 1999: Global water cycle. *Global Energy and Water Cycles,* K. A. Browning and R. J. Gurney, Eds., Cambridge University Press, 10–27.

——, K. Musiake, H. Matsuyama, and K. Masuda, 1995: Global atmospheric water balance and runoff from large river basins. *Hydrol. Processes,* **9,** 655–678.

Robock, A., C. A. Schlosser, K. Y. Vinnikov, N. A. Speranskaya, J. K. Entin, and S. Qiu, 1998: Evaluation of the AMIP soil moisture simulation. *Global Planet. Change,* **19,** 181–208.

——, K. Y. Vinnikov, G. Srinivasan, J. K. Entin, S. E. Hollinger, N. A. Speranskaya, S. Liu, and A. Namkhai, 2000: The Global Soil Moisture Data Bank. *Bull. Amer. Meteor. Soc.,* **81,** 1281–1299.

Row, L. W., D. A. Hastings, and P. K. Dunbar, 1995: *Terrainbase Worldwide Digital Terrain Data Documentation Manual, release 1.0.* National Geophysical Data Center, CD-ROM. [Available from National Geophysical Data Center, Mail Code E/GC, 325 Broadway, Boulder, CO 80303-3328; or online at http://www.ngdc.noaa.gov.]

Schemm, J., S. Schubert, J. Terry, and S. Bloom, 1992: Estimates of monthly mean soil moisture for 1979–1989. NASA Tech. Memo. 104571, National Aeronautics and Space Administration, Greenbelt, MD, 260 pp.

Schlosser, C. A., A. Robock, K. Y. Vinnikov, N. A. Speranskaya, and Y. Xue, 1997: 18-year land-surface hydrology model simulations for a midlatitude grassland catchment in Valdai, Russia. *Mon. Wea. Rev.,* **125,** 3279–3296.

——, A. G. Slater, A. Robock, A. J. Pitman, K. Y. Vinnikov, A. Henderson-Sellers, N. A. Speranskaya, and K. Mitchell, 2000: Simulations of a boreal grassland hydrology at Valdai, Russia: PILPS phase 2(d). *Mon. Wea. Rev.,* **128,** 301–321.

Sellers, P. J., F. G. Hall, G. Asrar, D. E. Strebel, and R. E. Murphy, 1992: An overview of the First International Satellite Land Surface Climatology Project (ISLSCP) Field Experiment (FIFE). *J. Geophys. Res.,* **97,** 18 345–18 371.

——, S. Los, C. Tucker, C. Justice, D. Dazlich, G. Collatz, and D. Randall, 1994: A global 1 by 1 degree NDVI data set for climate studies. Part 2: The generation of global fields of terrestrial biophysical parameters from the NDVI. *Int. J. Remote Sens.,* **15,** 3519–3545.

Shuttleworth, W. J., and Coauthors, 1984: Observations of radiation exchange above and below Amazonian forest. *Quart. J. Roy. Meteor. Soc.*, **110,** 1163–1169.

Smith, J. A., 1993: Precipitation. *Handbook of Hydrology,* D. R. Maidment, Ed., McGraw-Hill, 3.1–4.47.

Storck, P., and D. P. Lettenmaier, 1999: Predicting the effect of a forest canopy on ground snow accumulation and ablation in maritime climates. *Proc. 67th Western Snow Conf.,* Fort Collins, CO, 1–12.

Thornton, P. E., and S. W. Running, 1999: An improved algorithm for estimating incident daily solar radiation from measurements of temperature, humidity, and precipitation. *Agric. For. Meteor.,* **93,** 211–228.

Thorntwaite, C. W., and J. R. Mather, 1955: The world water balance. *Publ. Climatol.,* **8,** 1–86.

Todini, E., 1996: The ARNO rainfall–runoff model. *J. Hydrol.,* **175,** 339–382.

Vinnikov, K. Y., and I. B. Yeserpova, 1991: Soil moisture: Empirical data and model results. *J. Climate,* **4,** 66–79.

——, A. Robock, N. A. Speranskaya, and C. A. Schlosser, 1996: Scales of temporal and spatial variability of midlatitude soil moisture. *J. Geophys. Res.,* **101,** 7163–7164.

Willmott, C. J., C. M. Rowe, and Y. Mintz, 1985: Climatology of the terrestrial seasonal water cycle. *J. Climatol.,* **5,** 589–606.

Wood, E. F., D. P. Lettenmaier, X. Liang, B. Nijssen, and S. W. Wetzel, 1997: Hydrological modeling of continental-scale basins. *Annu. Rev. Earth Planet. Sci.,* **25,** 279–300.

——, and Coauthors, 1998: The Project for Intercomparison of Land-surface Parameterization Schemes (PILPS) Phase 2(c) Red–Arkansas River Basin experiment: 1. Experiment description and summary intercomparisons. *Global Planet. Change,* **19,** 115–135.